Taylor & Francis
Taylor & Francis Group

Automatika
Journal for Control, Measurement, Electronics, Computing and Communications

ISSN: (Print) (Online) Journal homepage: www.tandfonline.com/journals/taut20

Early detection of thermal image based T1 breast cancer using enhanced multiwavelet denoised convolution neural network with region based analysis

P. Geetha & S. UmaMaheswari

To cite this article: P. Geetha & S. UmaMaheswari (2024) Early detection of thermal image based T1 breast cancer using enhanced multiwavelet denoised convolution neural network with region based analysis, Automatika, 65:4, 1606-1620, DOI: 10.1080/00051144.2024.2413219

To link to this article: https://doi.org/10.1080/00051144.2024.2413219

Published online: 10 Oct 2024.

AUTOMATIKA
2024, VOL. 65, NO. 4, 1606–1620
https://doi.org/10.1080/00051144.2024.2413219

Early detection of thermal image based T1 breast cancer using enhanced multiwavelet denoised convolution neural network with region based analysis

P. Geetha[a] and S. UmaMaheswari[b]

[a]Department of Electronics and Instrumentation Engineering, SRM Institute of Science and Technology, Chennai, India; [b]Department of Electronics and Communication Engineering, SRM Institute of Science and Technology, Chennai, India

ABSTRACT
Medical Thermography image is used for the detection of breast cancer at an earlier stage. Thermography image shows the temperature change in the body due to cells. The metabolic rate of cancer cells is high compared to normal cells. A high metabolic rate increases the blood flow in cancer cells. High blood leads to changes in body temperature. The change in body temperature is used for cancer cell detection at an earlier stage. However, T1-stage cancer cells are smaller and have small temperature differences undetected with thermography. In this paper, a T1-stage cancer cell is heated by an external source; then, thermal images are acquired for earlier detection of small-size cancer cells. External heat source amplifies T1 stage cancer cell temperature. Amplified cancer cell images are analyzed using the proposed Multiwavelet-Deep Denoised Convolutional Neural Network (MWTDnCNN) algorithm for T1 cancer cell detection. Amplified T1 stage cancer cell has higher thermal conductivity (k) and heat capacity (Cp), which helps to detect T1 cancer cell tissue due to the enhanced pixel feature. The proposed MWTDnCNN algorithm has a T1-stage cancer cell detection accuracy of about 98% compared with traditional algorithms. The proposed MWTDnCNN algorithm detects T1-stage cancer of size 1.29 mm.

ARTICLE HISTORY
Received 5 January 2024
Accepted 23 September 2024

KEYWORDS
Multiwavelet denoised convolution neural network; thermal conductivity; heat capacity; region properties

1. Introduction

Cancer cells grow due to gene mutations in the breast tissues. Breast cancer develops in the lymph nodes. Breast cancer survival rates vary by cancer cell stages such as T1, T2, T3 and T4. Breast cancer detected at the early stage, i.e. T1 stage patients' survival rate is about 98–100%. T2-stage patients' survival rate is about 90–99%. T3-stage patients' survival rate is about 66–98% [1]. Breast cancer needs to be detected at an early stage to increase the patient's survival rates. Breast cancer is detected using various imaging modalities such as CT and MRI. CT and MRI image-based detection of T2 and T3 stages are more accurate. T2 stage detection has high false negatives when using CT and MRI images. Breast cancer cell stages are based on the cell count or size of the cancer cell. Cancer cell stage classification is performed using clinical and pathology methods. The clinical staging method is done before surgery. Pathologic staging is done after surgery. In 2018, the American Cancer Society defined the staging system. The breast cancer staging system is known as the TNM system, whereas T stands for tumour size, N for lymph nodes and M for metastasis (spread to distant sites). The T categories of breast cancer are determined based on tumour size. T followed by a number represents tumour size that has spread to the skin or chest wall or behind the breast. Big-size tumours or extensive spread are indicated through higher T values. TX indicates primary tumour, T0-No is the evidence of primary tumour, this is for the Carcinoma in situ (DCIS or Paget's disease of the breast without associated tumour mass), and T1 has substages such as T1a, T1b and T1c. The tumour is 2 cm (3/4 inch) or less in diameter. T2: Tumour is more than 2 cm, not more than 5 cm (2 in.) in diameter. T3: The tumour is more than 5 cm in diameter. T4: Any size tumour that extends into the skin or chest wall and has sub-stages such as T4a, T4b, T4c and T4d, including breast inflammation.

Breast cancers are detected using physical breast cancer screening, sonography, mammography and MRI. A physical Breast cancer screening test is a self-examination method. Breast examination at the clinic is performed using various imaging modalities such as sonography, mammography and MRI. Clinical breast examination (CBE) is the primary method for identifying cystic breast lesions [2]. CBE has low sensitivity and is unreliable in the detection of malignancy. Biopsy is done after medical image analysis [3]. Mammography uses X-rays for breast abnormality diagnosis. A mammogram is a quick and common means of detecting breast cancer. However, mammography has low spatial resolution and requires significant storage space. Breast MRI [4] is recommended by the American Cancer Society for women at high risk of

CONTACT P. Geetha geethaphd2020@gmail.com Department of Electronics and Instrumentation Engineering, SRM Institute of Science and Technology, Kattankulathur, Chennai 603203, India

cancer; MRI scanning cost is high, the machine is non-portable, images with low specificity, and consumes more time. Sonography [5], or breast ultrasound, generates sound waves, passes through the organs with the help of a transducer, and provides low-resolution and low-contrast images. Positron emission tomography (PET) [6], single-photon emission computed tomography (SPECT), and mammography are nuclear imaging modalities. In a PET scan, fluorodeoxyglucose (FDG) is used as a radioactive tracer, which is injected into an arm vein and targets the malignant tissue. PET imaging is independent of breast density, prior surgery or radiation therapy. PET images have limited resolution and imaging capabilities. Breast thermogram images are used to prevent the spread of cancer. Detection of breast tumours in women with dense breasts is a challenging task.

Infrared (IR) cameras are used in thermography to acquire temperature profiles of the breast. The temperature distribution on the breast surface is used for the detection of cancer. The IR image distinguishes normal and uncontrolled cancer cell growth through temperature variations. Cancer cells have a higher metabolic rate and greater blood flow in the surrounding tissue. A higher metabolic rate increases the heat in the breast's cancer tissue regions. The breast heat patterns are used for the diagnosis of breast cancer. Thermal image processing is a non-invasive method for detecting small breast tumours due to its non-ionizing nature and ability to distinguish benign from malignant lesions. It provides physiological information about vascularity and metabolism, effectively detecting cancer in women with dense breast tissue. Thermal image-based techniques must be improved due to the early detection rates, i.e. the T1 stage. Breast thermography is used to detect breast cancer in its initial stages. Breast thermography is a painless, non-invasive procedure.

When thermography produces heat and cold in the affected area, cancer cells are identified using infrared imaging technology. The cancer area becomes warmer than other areas because the growth of cancer cells requires higher blood flow. The development of cancer cells can be detected in a thermogram after two years, whereas mammography can only do so after eight years [7]. Thermal imaging detected the cancer cells at an early stage. In thermography, red and yellow represent warmer colours, whereas green and blue represent cooler colours. Thermal breast cancer images are of low resolution. Due to low resolution, researchers apply different and transfer learning models for the detection of cancer cells. Instead, they require an infrared camera with high resolution. A multiresolution convolutional neural network is required to detect cancer cells from thermal images.

1.1. Research gap

Figure 1 shows the research gap in breast cancer detection. Breast cancer cells are detected through mammograms after 4–10 years. However, Thermal imaging can detect cancer cells from the second year onwards.

Mammography, ultrasound and MRI scans can detect breast cancer in the 5th year. The above imaging methods have certain drawbacks, such as not being recommended for lactating or pregnant women and never being advisable for women in all age groups. However, thermography is a non-invasive, economical and radiation-free method. Thermography is useful for detecting breast cancer at earlier stages [9]. Breast cancer is detected through five different views of breast images using a convolutional neural network [10]. Breast cancer is detected through static and dynamic infrared thermography with machine learning techniques such as support vector machine and k-star algorithm [11]. This paper proposes cancer cell detection below two years, i.e. T1 stage using thermal imaging using hybrid algorithms such as wavelet and convolution neural networks.

1.2. Contributions

This paper proposes a multiwavelet deep denoised convolutional neural network (MWTDnCNN) for detecting breast cancer cells below 2 years using

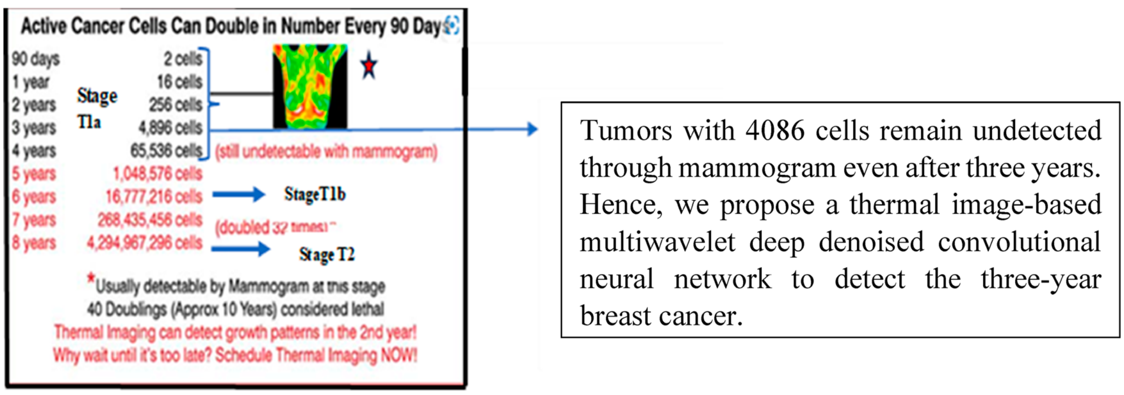

Figure 1. Research Gap in identification of breast cancer cells [8].

heat-amplified cancer cell thermal images. This is achieved through external heat source amplification of T1 stage cancer cells in the breast region and obtained the thermal images for detection of cancer cells below 2 years.

1. To enhance the boundary and edges of cancer cells in thermal images, hybrid of Haar wavelet transform and symmetric wavelet basis function is proposed. The perspective projection property of symmetric wavelet basis function enhances the region of cancer cell in the heat amplified cancer cell thermal images.
2. To differentiate cancer cells in the thermal image, Kullback–Leibler is proposed, which effectively differentiates cancer and normal cells based on probability variation, and then filtered through the proposed MWTDnCNN algorithm.
3. To classify cancer cell growth patterns from normal cells, the breast cancer image is segmented through adaptive binary thresholding image segmentation, and region properties are extracted and locate the cancer cells in the heat amplified cancer cell thermal images.

Section 2 of this research describes state-of-the-art technology, and Section 3 describes the proposed methodology for finding breast tumours. Stages T0, T1 and T2 results and discussions are presented in Section 4. Conclusion and future work are covered in Section 5.

2. Literature survey

Several studies have explored the application of image processing methods for breast cancer detection using thermal imaging. A multi-input convolutional neural network (CNN) was used in [12] to categorize breast images into healthy and diseased categories based on various lateral angles. CNNs automatically extract features from breast thermal images. In another study [13], a non-invasive method for breast cancer detection, which is radiation-free, was used. The Levenberg–Marquardt algorithm is used for breast tumour detection. Still, efficiency should be improved by automating the breast geometry determination procedure. In [14], healthy and unhealthy breast cancer were classified using the Shannon entropy, a measure of uncertainty in a dataset, in the left and right breast images. This method has low sensitivity to thermal images and needs enhancement algorithms for early detection of breast cancer.

In [15], feature aggregation strategies were utilized to overcome the problem of identical images in transfer learning deep models for breast cancer classification. However, the potential of additional investigation to address class inequalities within the dataset is promising. Despite the drawbacks of a small dataset, [16] used machine learning methods and categorized the breast tumour images such as normal, benign and cancerous images. Similarly, [17] used dynamic infrared thermography for discrimination of benign and malignant tumours through combining CNN and Bayes algorithm. In [18], researchers investigated the predictive potential of biomarkers, including hyperglycaemia, resisting and BMI for breast cancer. Authors used SVM, RF and decision tree models for detection of the breast cancer. On the other hand, adding more biomarker data improves prediction accuracy.

The use of a 3D printer in [19] for the assessment of tumour depth, ranging in size from 5 to 25 mm, and considering tissue mechanical qualities, presents a promising future for accurate diagnosis and treatment planning. The statistical analysis of tumour breadth and volume is crucial. Dey et al. [20] attempted to distinguish between malignant and healthy breast images using a pre-trained Dense Net 121 model. The issues of class imbalance with minority cancer classes are the major problem. Macedo et al. [21] concentrated on classifying cysts, benign and malignant breast lesions through shape information, which is extracted using Zernike and Haralick texture moments. This method is suitable for small datasets.

Thermal sensitivity camera images were used [22] for the identification of breast cancer using deep learning models, a promising avenue for future research. Ghayoumi Zadeh et al. [23] Multilayer perceptron for classification, self-organizing maps for clustering suits for small databases. In [24], pre-processing, segmentation, feature selection and extraction were used for categorization of thermos vascular breast stages. However, there were differences in the outcomes between cases of right and left breast cancer. Malignant tumour images were segmented using an ROI image segmentation technique in [25], and additional statistical means-based tumour width analysis was performed. In [26], breast geometry from 3D scanner used for the quantification of the thermal properties of triple negative breast cancer. For breast cancer detection, vasculature and blood flow in the breast are analyzed. In [27], the World Cup optimization technique and neural network model were used for breast cancer detection. In [28], the Grey Wolf Optimisation (GWO) method optimizes the multilayer perceptron neural network and improves the prediction accuracy. In [29], convolutional neural network and the satin power bird optimizer (SBO) improve the convergence rate during breast cancer prediction.

3. Methodology

Multiwavelet deep denoised convolutional neural network (MWTDnCNN) is used to detect T1 stage breast cancer cells from heat-amplified cancer cell thermal images. The amplified T1 stage cancer cell thermal images of breast region process with Haar and symmetric basis for removing artifact in the boundary regions. Next, Kullback Leibler divergence is used for the differentiation of cancer and non-cancer cells. Then, applied with the proposed MWTDnCNN algorithm for denoising the thermal image, adaptive binary thresholding image segmentation is performed for the classification of stages of cancer in the heat-amplified cancer cell thermal images.

Figure 2 shows the proposed methodology to detect the cancer cells in a breast thermogram image. Initially, the image is converted into a YCbCr colour image. Then Haar wavelet transform with symmetric basis function is applied to each decomposed image and removes the boundary artefacts. Then, the Kullback–Leibler divergence algorithm is used to improve the perspective projection of cancer and non-cancer cells through the probability of pixel variation. The proposed MWTD-nCNN algorithm denoises the heat-amplified cancer cell thermal images. Next, an adaptive binary image segmentation algorithm is used for the classification of the T1 cancer cell. Then, the region properties are extracted from the segmented breast image, and the accumulation of T1 cancer cells is located. Figure 3 shows the flow diagram and pseudocode of a proposed approach.

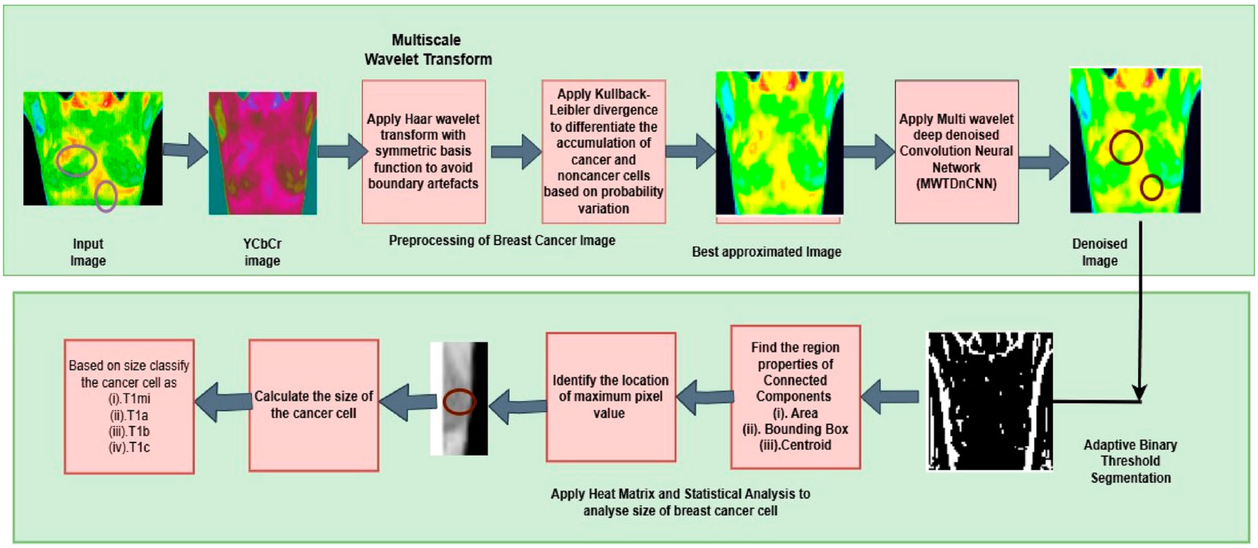

Figure 2. Proposed MWTDnCNN Algorithm to detect Breast Cancer at Early Stage.


```
Procedure BreastCancerDetectionThermography(thermal_image):
  // Convert RGB thermal image to YcbCr image
  ycbcr_image = ConvertRGBtoYCbCr(thermal_image)
  // Apply wavelet transform to each band
  for each band in ycbcr_image:
     wavelet_transform(band)
  // Apply Kullback-Leibler Divergence (KLD) to choose the best level
of approximation for each channel
  best_approximation = ChooseBestApproximation(ycbcr_image)
  // Deep denoised convolutional neural network (CNN) for image
improvement
  improved_image = DeepDenoisedCNN(best_approximation)
  // Segment breast image using adaptive binary thresholding
  segmented_image = AdaptiveBinaryThresholding(improved_image)

  // Discover region attributes of linked components
  region_attributes = DiscoverRegionAttributes(segmented_image)

  // Create heat matrix using highest temperature recorded in specific
area
  heat_matrix = CreateHeatMatrix(region_attributes)

  // Determine damaged area and size of cancer cell
  damaged_area, cancer_cell_size =
DetermineDamagedAreaAndCancerCellSize(heat_matrix)
  // Classify cancer cell size

  classification = ClassifyCancerCellSize(cancer_cell_size)

  return classification
```

Figure 3. Flow diagram and Pseudocode of proposed MWTDnCNN Algorithm.

3.1. Experimental setup

The experimental setup for the thermography of a breast image is shown in Figure 4. The MCP electric heat belt holds the patient is back together. The heat is dynamically generated through the belt and transferred to the breast region. The image is captured over 90 days using a thermal camera at various temperatures with heat-amplified cancer regions. The amplification is performed using the MCP electric heat belt. Utilizing ultra-heat technology, the pad reaches the maximum temperature. Thermal imaging of breast cancer cells shows temperature variations above room temperature. Temperature changes depending on tumour size, metabolic activity and physiological variations. The temperature of malignant tissue in the breast is a few tenths of a degree Celsius higher than the surrounding healthy tissue. We have set the temperature between 38.2 and 42.5°C, which is higher than the typical room temperature, i.e. 33°C [3031]. Then, heat-amplified cancer tissue regions are acquired with the thermal camera for image analysis using the proposed MWTDnCNNalgorithm.

3.2. Convert RGB to YCbCr image

The YCbCr model is called the YUV model. YCbCr has advantages over RGB thermal image processing, such as (i). Separation of luminance and Chrominance (ii). Reduced in size. (iii). Improved Compression. (iv). Increased Dynamic Range. (v). Reduced noise. In the YCbCr model, the Y component represents an 8-bit greyscale image with the values 0 (black) to 255 (white) and represents the luminance and brightness of an image. Cb and Cr are used as representations for the 8-bit colour difference signals. Equations (1)–(3) show the conversion of an image. Figure 5 shows the original RGB thermal image and YCbCr thermal image.

$$Y = 0.299R + 0.587G + 0.114B \tag{1}$$

$$Cb = -0.169R - 0.331G + 0.5B + 128 \tag{2}$$

$$Cr = 0.5R - 0.419G - 0.081B + 128 \tag{3}$$

3.3. Multiscale wavelet transform

Multiscale wavelets are transformed to analyse the image in a multiscale frequency domain and decompose an image into different frequency bands, each band containing information of different scales. Multiscale wavelet transform is used for denoising, compression and feature extraction. Multiscale wavelet transforms consist of a 4-level decomposition of the Haar wavelet transform and symmetric basis function to differentiate small changes in amplified cancer cell breast thermal image due to orthogonal property. To improve breast cancer detection accuracy, perspective projection of T1-stage cancer cells is performed using the Haar multiresolution transform, which extracts coarse- and fine-scale cancer cells that are small in count.

The multiscale wavelet transform is applied to two-dimensional heat-amplified cancer cell thermal images. The decomposition is performed independently in each dimension, resulting in four frequency sub bands at each level such as LL (low-low), LH (low-high), HL (high-low) and HH (high-high). The image is I(x, y), where x and y represent the spatial coordinates. The wavelet decomposition is performed through applying

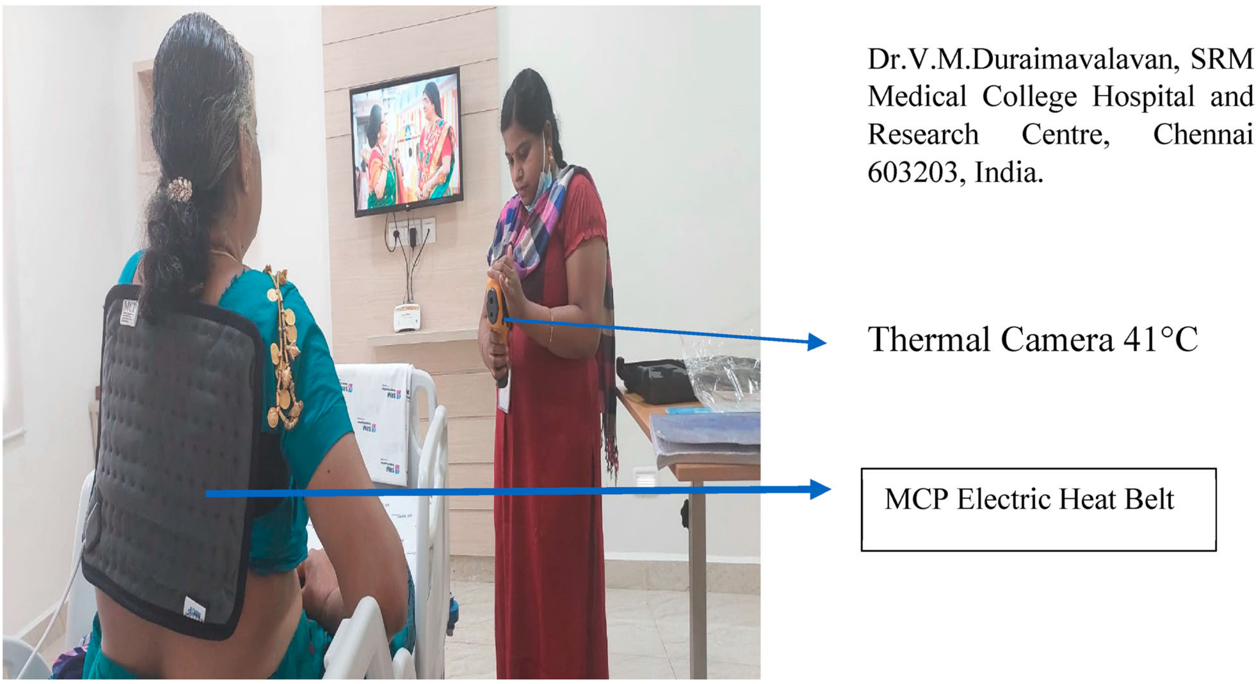

Figure 4. Experimental Set up for heat amplified cancer cell using heating pad and thermal image acquisition.

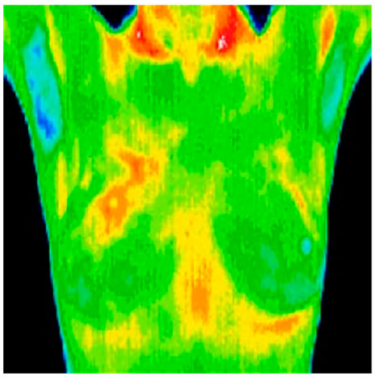

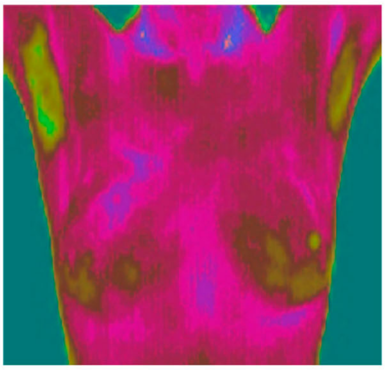

Figure 5. (a) Original RGB thermal image. (b) YCbCr thermal Image.

2D separable convolution, which consists of a pair of filters h and g, in both horizontal and vertical directions. The filters h and g are called the scaling and wavelet filters, respectively.

The multiscale wavelet transform is as in equation (4).

$$I_j = I * \emptyset_j + W_j \tag{4}$$

where I_j represents the image at scale j, $\emptyset_j$ represents the low-pass filter heat amplified cancer cell thermal images at scale j, W_j represents the high-pass filter heat amplified cancer cell thermal images at scale j, $*$ denotes convolution and the subscript j denotes the level of decomposition.

The low-pass filtered image $\emptyset_j$ is obtained through convolution of input image I with 2D separable filter h at scale j, then performed the subsampling through the factor 2↑j in both horizontal and vertical directions in the heat amplified cancer cell thermal image. The low pass filtered heat amplified cancer cell thermal images is represented in equation (5)

$$\emptyset_j(x, y) = (h * I)(2 \uparrow jx, 2 \uparrow jy) \tag{5}$$

The high-pass filtered image W_j is obtained the convolution of the input thermal image I with a 2D separable filter g at scale j, then performed the subsampling through the factor of 2↑j in both horizontal and vertical directions heat amplified cancer cell thermal images. The high pass filtered heat amplified cancer cell thermal images is represented in equation (6).

$$W_j(x, y) = (g * I)(2 \downarrow jx, 2 \downarrow jy) \tag{6}$$

Wavelet decomposition is represented as a tree structure, where top of the tree is the input image I, and each level of the tree corresponds to different scale of wavelet decomposition.

The wavelet reconstruction is represented in equation (7)

$$I = \sum_j I_j \tag{7}$$

where I_j represents the heat amplified cancer cell thermal images at scale j, and the reconstruction involves adding up the high-pass filtered heat amplified cancer cell thermal images and the low-pass filtered heat amplified cancer cell thermal images at the highest level of decomposition. The reconstruction process involves up sampling the high-pass filtered heat amplified cancer cell thermal images by a factor of 2 in both horizontal and vertical directions, and convolute with the corresponding wavelet filters and reconstruct the thermal image I. The low-pass filtered heat amplified cancer cell thermal images at the highest level of decomposition is up sampled and convolute with corresponding scaling filter, and obtain the reconstructed thermal image. To eliminate the boundary effects in thermal breast cancer image, symmetric basis function decomposes the breast cancer image and accurately analyse the local features, without artificial discontinuities at the boundaries. This method provides smooth variation at the edges and boundaries in heat amplified cancer cell thermal images.

3.4. Kullback Leibler Divergence (KLD) for best approximation of heat enhanced thermal images

By computing KLD in each subband, then apply Kullback–Leibeler [32] divergence, and determine the optimal approximation level for the heat amplified cancer cell thermal image. The best approximation is selected based on maximum KLD value. Hence, KLD, is known as relative entropy, which is a metric for comparing two probability distributions. KL divergence is defined as given two discrete probability distributions such as P(x) and Q(x) over the same sample space x in equation (8).

$$KL(P||\mathrm{Q}) = \sum \mathrm{xP(x)log}\left(\frac{P(x)}{Q(x)}\right) \tag{8}$$

where log is the natural logarithm. KL divergence is a non-negative quantity that is equal to zero, if and only if P and Q are identical, undefined if P(x) is zero for some x, where Q(x) is nonzero. Intuitively, KL divergence measures the amount of information lost using Q to approximate P. KL is interpreted as the average amount of extra bits required to encode samples using P, code optimized for Q, instead of a code optimized for P. The KL divergence is not symmetric, i.e. KL(P || Q) is not necessarily equal to KL(Q || P). In general, KL (P || Q) measures the difference between the "true" distribution P and the "approximating" distribution Q, whereas KL(Q || P) measures the difference between the "approximating" distribution Q and the "true" distribution P.

3.5. Deep denoised convolution neural network (DnCNN) for heat amplified thermal images

Heat amplified cancer cell thermal images has temperature variations, sensor noise, ambient conditions, and the sensitivity of objects, which are the causes of noise in thermal images. A low-sensitivity object has more noise in thermal image and will reflect more heat. Parameter optimization in denoising technique is difficult and more time consuming. Hence, the parameters of denoising models are manually selected. The deep denoised convolution neural network (DnCNN) [33] enhances heat amplified cancer cell thermal images. DnCNN model is represented as in equation (9) and x is an image, y is a noisy image with additive white gaussian noise "v"

$$y = x + v(Additive\ White\ Gaussian\ noise) \tag{9}$$

Receptive field of DnCNN with (3 × 3 Conv Network) with depth d is (2d + 1) x(2d + 1)

$$F(y) = x \tag{10}$$

In equation (10) $F(y)$ is a clean latent image

$$R(y) \simeq v \tag{11}$$

Equation (10) and (11) represents residual mapping of clean and noisy image.

$$x = y - R(y) \tag{12}$$

DnCNN consist of four types of layers convolution with Relu Layer 3 × 3 with 64 feature maps designed for gray scale image. The four layers are Conv layer, Batch Normalization Layer, and Relu Layer and last layer is regression layer, which is used for reconstruction of the output image. Figure 6 shows DnCNN layers and its operations.

3.6. Adaptive binary threshold

Adaptive Binary thresholding separates pixels in an image into two categories: foreground and background. Foreground and background separation is performed through the threshold value of pixel intensity, and any pixel above the threshold is considered the foreground. In contrast, any pixel below the threshold value is considered as the background of an image. In adaptive binary thresholding, the threshold value is not fixed; however, it is adjusted dynamically based on the local characteristics of the image. This is done through the threshold value calculation for each pixel based on the intensity values of its neighbouring pixels. The threshold value is usually set to be the average intensity value of the neighbouring pixels.

Let f(x, y) be the intensity value of a pixel at position (x, y) in the input image. Calculate the threshold value T(x, y) for each pixel using the local mean method as in equation (13)

$$T(x, y) = mean(f(x-k, y-k) \\ \ldots .f(x+k, y+k))$$

$$T(x,\ y) = mean(f(x-k,\ y-k),\ \ldots,\ f(x+k,\ y+k)) \tag{13}$$

where k is the half-size of the local window used for calculating the mean, and f(x-k, y-k), … , f(x + k, y + k) are the intensity values of the pixels within the local window centred at (x, y).

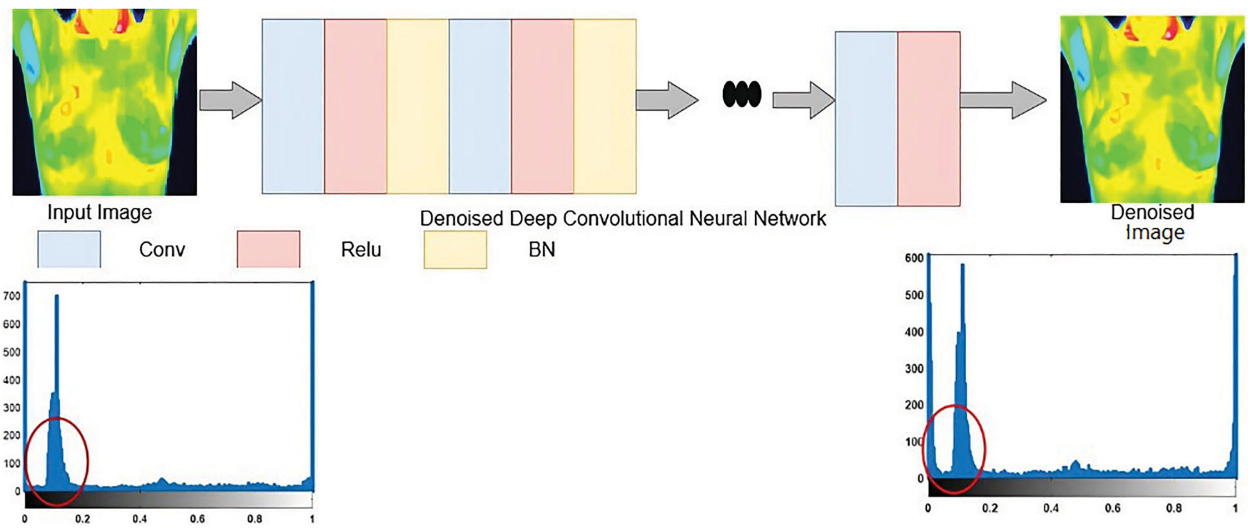

Figure 6. Denoised[Q9] image for heat amplified thermal image.

Once the threshold value T(x, y) is computed for each pixel, generates the binary image g(x, y) in equation (14)

$$g(x,y) = \begin{cases} 1, & f(x,y) \geq T(x,y) \\ 0, & f(x,y) < T(x,y) \end{cases} \quad (14)$$

where g(x, y) is the binary image, with white pixels represents the foreground and black pixels represents the background.

3.7. Statistical properties of connected components of segmented heat amplified thermal image

Connected components are represented mathematically using binary images, where pixels inside the component are assigned a value as 1 and pixels outside the component are assigned a value as 0. From this binary image, various region properties of the connected components are computed. The area of the connected component is calculated as the sum of all the pixels in the binary image, which is given in equation (15):

$$Area = \sum g(x,y) \quad (15)$$

where $\sum$ denotes the sum over all pixels (x, y) in the binary image.

The bounding box of the connected component is the smallest rectangle that encloses all the pixels in the component. Compute the bounding box as in equation (16).

Let (x1, y1) be the top-left corner of the bounding box, and (x2, y2) be the bottom-right corner of the bounding box. Then, calculate

$$\begin{aligned} x1 &= min\{x|g(x,y) = 1\} \\ y1 &= \min\{y|g(x,y) = 1\} \\ x2 &= max\{x|g(x,y) = 1\} \\ y2 &= \max\{y|g(x,y) = 1\} \end{aligned} \quad (16)$$

In other words, smallest and largest x and y coordinates of the pixels in the binary image that have a value of 1.

The centroid of the connected component represents the average position of all the pixels in the component and calculated the centroid as below:

Let (cx, cy) be the centroid of the connected component shown in equation (17)

$$\begin{aligned} cx &= \left(\frac{1}{A}\right) * \sum x * g(x,y), \\ cy &= \left(\frac{1}{A}\right) * \sum y * g(x,y) \end{aligned} \quad (17)$$

where $\sum$x and $\sum$y denotes the sum over all x and y coordinates of the pixels in the binary image with value of 1. The centroid (cx, cy) represents the centre of the connected component.

4. Results and discussions

Temperature fluctuations in the skin region are easily detected using thermal imaging. Thermal imaging is effective in breast cancer detection at the early stage when compared to other imaging modalities. Figure 7 shows the thermography of a 37-year-old patient; thermography images were obtained every 3 months. It indicates a temperature change in a woman's upper right breast in the image's baseline. Hence, the screening was carried out every 90 days. After a year, the patient's mammogram revealed a 1 mm T1 cancer cell and a biopsy was performed.

Figure 7 shows the 37-year-old patient heat amplified cancer cell thermal images (a). Baseline – slight increase in temperature in upper right breast (b). 3 months-increase temperature (e). 12 months 1 mm breast cancer identified. Figure 8 shows the results of the Heat amplified cancer cell thermal breast image after denoising. Figure 8 shows the pixel differences magnified.

4.1. KL divergence

KL divergence estimates the best approximated image and denoise the Heat amplified cancer cell thermal images image through maximum pixel variation. Figure 9 shows the best approximated heat amplified

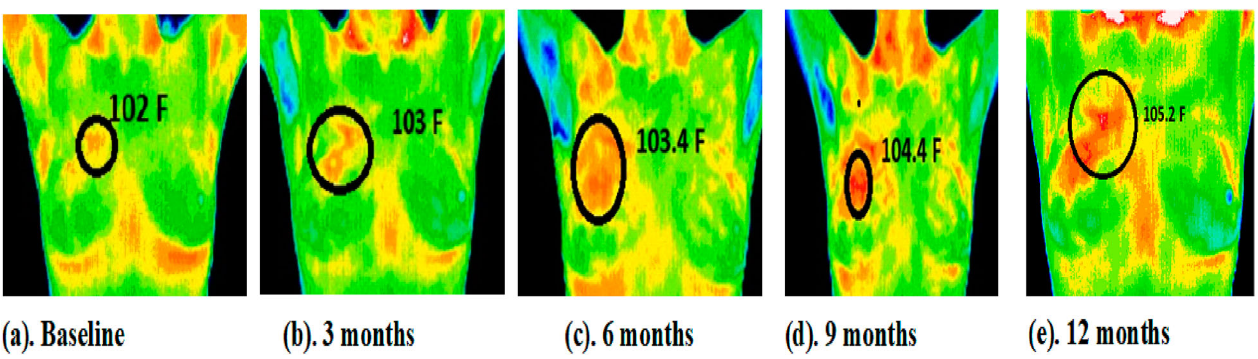

Figure 7. Breast thermogram.

Input Image	YCbCr Image	Best approximated image	Denoised Image
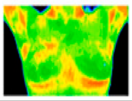	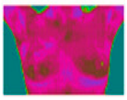	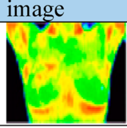	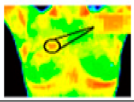
(i).input image(baseline)	(ii).Converted Color image	(iii).Best approximated	(iv).Denoised Image
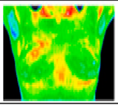	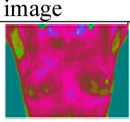	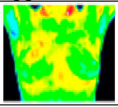	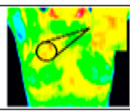
(i).input image(3rd month)	(ii).Converted Color image	(iii).Best approximated	(iv).Denoised Image
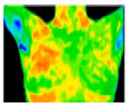	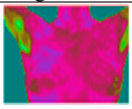	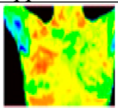	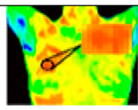
(i).input image(6th month)	(ii).Converted Color image	(iii).Best approximated	(iv).Denoised Image

Figure 8. Results obtained through MWTDnCNN.

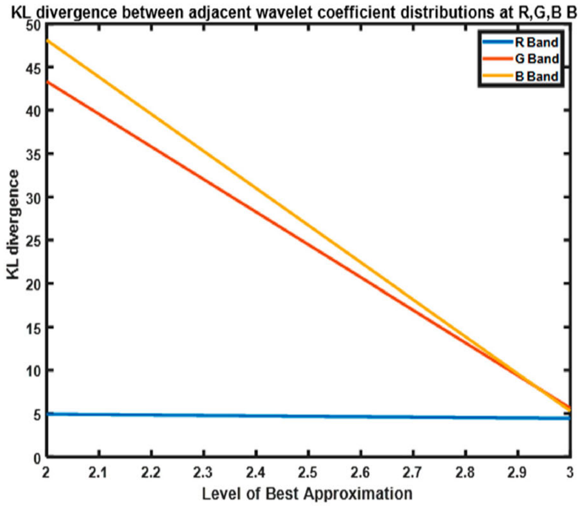

(a).Base(R=4.9,G=42.5,B=48.5)

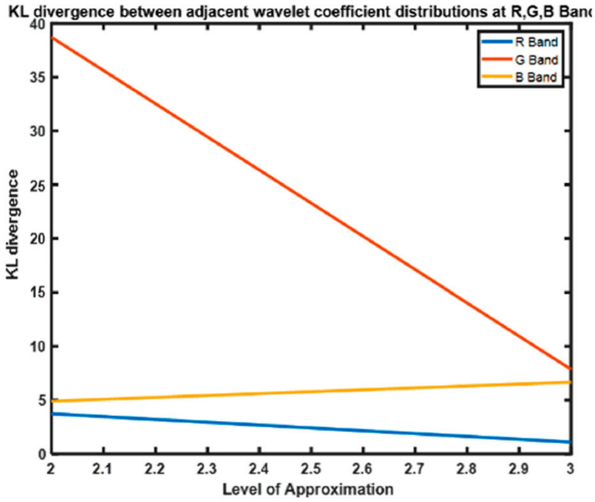

(b).3 Months(R=4.5,G=4.9,B=38.5)

Figure 9. Best approximation based on KL Divergence of heat amplified thermal image. (a) Base(R = 4.9,G = 42.5,B = 48.5). (b) 3 Months(R = 4.5,G = 4.9,B = 38.5).

Table 1. Best Optimized Parameter of heat amplified thermal Images.

Wavelet Type	Decomposition level	Threshold Value	PSNR Value (decibel)
Haar	Level 1	1	20.53
Haar	Level 2	5	25.56
Haar	Level 3	10	45.87
Haar	Level 4	15	42.86

cancer cell thermal images, and Table 1 shows the different levels of approximation and their peak signal-to-noise ratio (PSNR) values.

The optimal set of parameter values is level 3 decomposition, with a threshold value of 10 and PSNR value is high among the original and approximated image. Hence, a level 3 approximated image is selected and detected the T1 stage cancer cells.

Table 2 shows the heat capacity and thermal conductivity of R,G,B pixel values based on the following equations (18)–(21).

$$Heat\ Capacity(Cp) = 3399.3712 + 0.0275 * R + 1.0868 * G - 0.1836 * B(Normal\ Cell) \tag{18}$$

$$Heat\ capacity(Cp) = 2997.9389 + 2.6619 * R - 0.0866 * G - 0.2158 * B(Cancer\ Cell) \tag{19}$$

$$Thermal\ Conductivity(k) = 0.031 + 0 * R + 0.0001 * G + 0 * B(Normal\ Cell) \tag{20}$$

$$Thermal\ Conductivity(k) = -0.0238 + 0.0002 * R + 0 * G + 0.0001 * B(Cancer\ Cell) \tag{21}$$

Table 2 is related to breast cancer cell and the heat capacity and thermal conductivity of the R,G,B pixels due to the rapid growth of cancer cells. Breast cancer

Table 2. Heat capacity and thermal conductivity of real breast image using R,G,B values of Cancer and Non cancer cells.

R-Component of Heat amplified cancer cell thermal image	G-Component of Heat amplified cancer cell thermal image	B-Component of Heat amplified cancer cell thermal image	Heat Capacity (Cp)	Thermal Conductivit y(k)
12 Months				
230	198	92	3603.991	0.0508
255	193	95	3598.694	0.0503
245	188	75	3596.657	0.0498
249	190	50	3603.531	0.05
246	197	25	3615.646	0.0507
255	167	45	3579.617	0.0477
240	155	56	3564.144	0.0465
245	179	45	3592.384	0.0489
240	150	65	3557.057	0.046
9 Months				
245	194	90	3613.882	0.0342
230	182	84	3576.288	0.0306
225	160	82	3565.315	0.0294
210	140	89	3525.608	0.0271
216	182	94	3536.863	0.0288
220	178	96	3547.425	0.0298
227	182	92	3566.575	0.0308
220	186	94	3547.164	0.0296
6 Months				
225	192	92	3597.333	0.0502
255	188	90	3594.178	0.0498
240	185	70	3594.177	0.0495
230	186	45	3599.579	0.0496
244	195	20	3614.335	0.0505
250	160	35	3573.708	0.047
245	150	56	3558.847	0.046
235	170	35	3584.164	0.048
230	145	60	3552.266	0.0455
Base Image				
127	114	81	3511.887	0.0097
126	115	77	3513.681	0.0091
84	119	91	3514.303	0.0021
109	88	20	3494.335	−1.7E-18
84	40	10	3443.317	−0.006
109	113	29	3519.853	0.0009
124	112	36	3517.893	0.0046
120	102	25	3508.935	0.0027
104	51	57	3447.193	0.0027
3 months				
234	182	81	3588.732	0.0311
255	185	88	3591.285	0.036
231	165	67	3572.745	0.0291
220	180	34	3594.803	0.0236
244	190	10	3610.737	0.026
245	150	29	3563.804	0.0281
226	145	38	3556.195	0.0252
227	162	26	3576.902	0.0242
228	164	54	3573.962	0.0272

differs from normal breast tissue. Cancer cells divide more quickly and have a greater metabolic rate, which can alter their physical characteristics, such as their thermal conductivity and heat capacity. According to the statement, larger pixel values were seen at 3, 6, and 12 months compared to a baseline image, indicating that the heat capacity and thermal conductivity of the R, G and B pixels in breast cancer images increased over a period of time.

Figure 10 shows the region properties of heat amplified cancer cell thermal images such as boundary, centroid and area of baseline, 3, 6, 9 and 12 months. Breast cancer is a complex disease that is diagnosed based on various characteristics of the affected region. A breast cancer image's boundary refers to the lesion's margins and boundaries. The area of a breast cancer comprises of the size, shape, position and density of the malignant tissue. The centroid denotes the geometric centre of the tumour.

Figures 11 and 12 display the confusion matrices and statistical analysis of Heat amplified cancer cell thermal images, which are summarized in Table 3. The confusion matrix is obtained through comparison of the predicted tissue with the actual tissue statistical analysis includes performance metrics such as accuracy, precision, recall and F-measure. Based on these metrics, recognition accuracy is detected for the breast cancer at earlier stage. Traditional techniques for breast cancer detection take up to 10 years, however breast cancer cells multiply rapidly over a 90-day period. Therefore, thermogram screening of a 37-year-old woman within one year is analysed for the T1 stage cancer. Similarly, 50

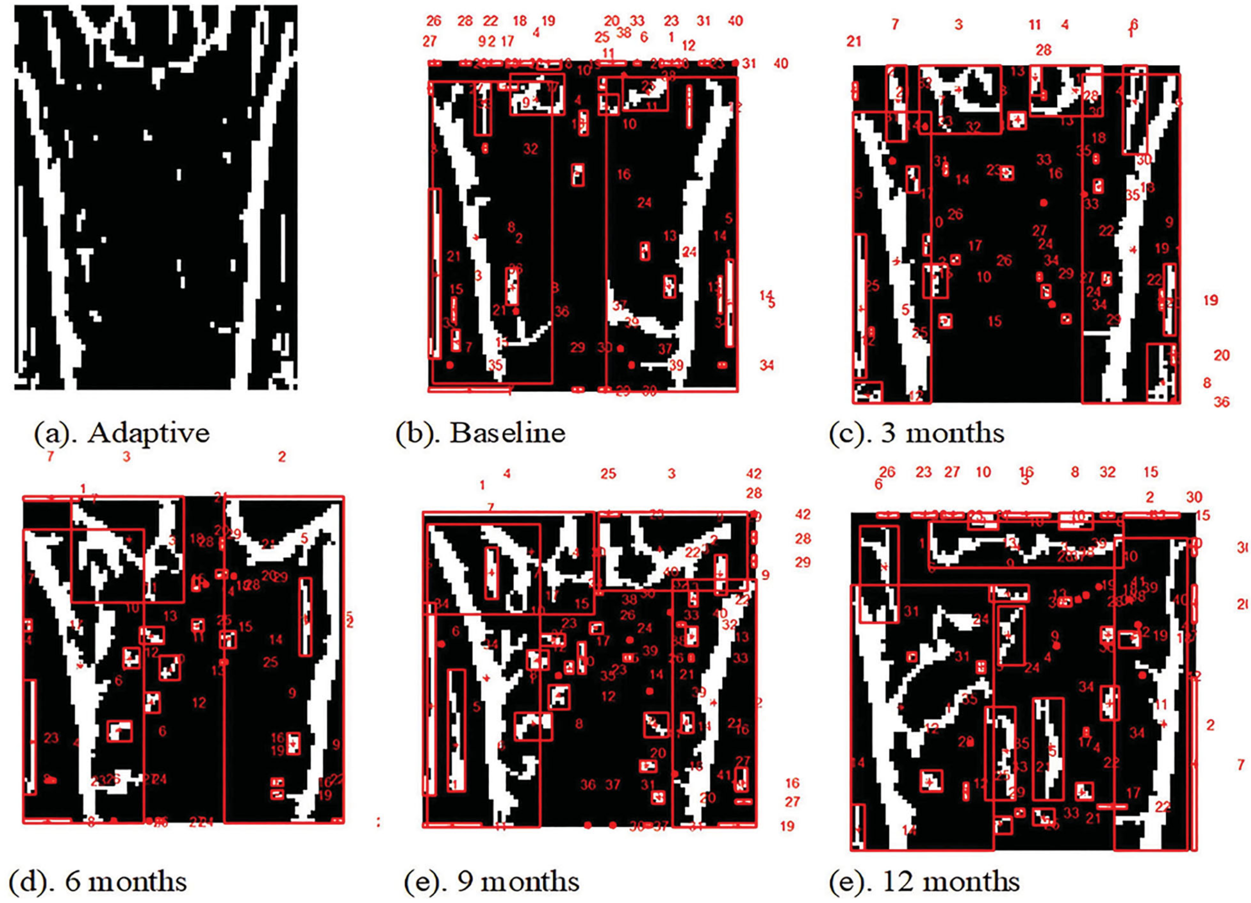

Figure 10. Region properties of breast cancer heat amplified cancer cell thermal images.

T1 stage cancer patients were analysed and achieved a recognition accuracy of 98% for T1stage cancer patient.

4.2. *Size of a breast cancer*

Early breast cancer detection is essential for successful management and therapy. Physicians utilize computer-aided detection tools and automatically measure the size of the breast cancer in addition to manual measurements. The proposed MWTDnCNN method enhances the area with the greatest temperature value of T1 cancer cells. The MWTDnCNN identifies the cancer location automatically based on the highest pixel intensity. MWTDnCNN method is effective for precise cancer size measurements and shown in Figure 13. Table 4 displays the actual size and stage of the breast cancer. Table 5 compares the thermal breast detection using different imaging modalities.

1. Arrange the Region Properties of an image such as area, centroid and bounding box in highest to lowest.
2. Crop the largest bounding box of an image.
3. Then assign the camera calibration factor as 0.025 for each pixel.
4. Calculate size = width$*$pixel$*$height$*$pixel
5. Based on size, analyse the tumour stage

Hence, the estimated size of a tumour is 1.29 mm and it indicates the stage is T1a. But the actual size of the tumour is 1 mm.

Table 6 shows the comparison of existing and the proposed methods based on the precision, recall and accuracy. The proposed MWTDnCNN method tracks temperature changes over 90-day period in patients with a history of breast cancer and T1 stages cancer cells. MWTDnCNN method has greater accuracy and sensitivity, and detects T1a stage breast cancer cell of size below 1.29 mm in size.

5. Conclusion

Breast cancer is detected using different methods such as mammograms, ultrasound imaging and MRI techniques. Thermography is used for the identification of breast cancer by detecting the highest temperature variation among the normal and cancer cells of the breast region. The cancer cell has increased blood flow in the cancerous regions. Kullback–Leibler divergence eliminates undesired noise in heat-amplified

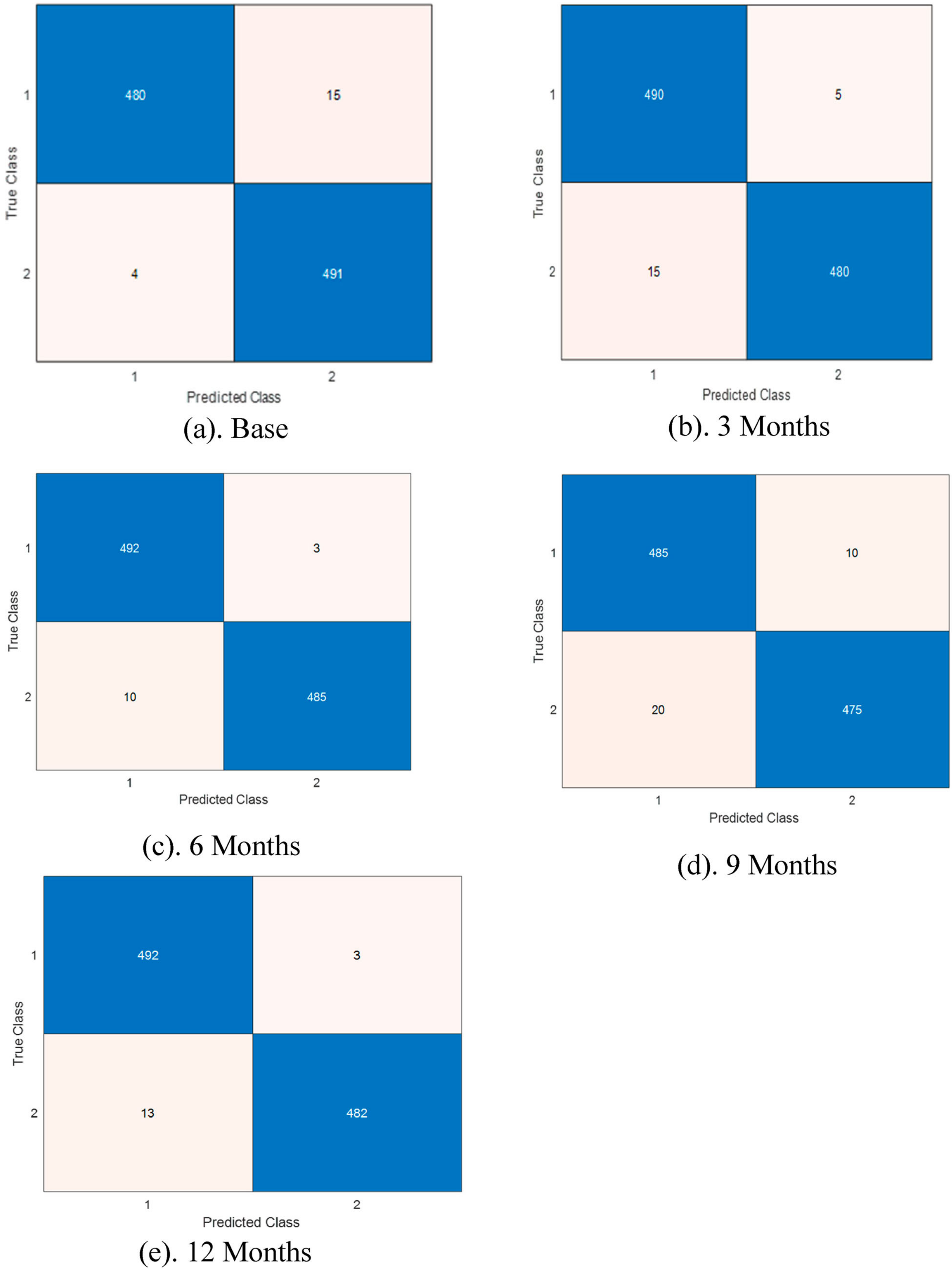

Figure 11. Confusion Matrix of Base, 3 Months, 6 Months, 9 Months, 12 Months of Heat amplified cancer cell thermal images Region.

cancer cell thermal images. Then, the Multiwavelet-based Deep Denoised Convolutional Neural Network (MWTDnCNN) is applied, enhancing the T1 stage cancer cell regions. The T1 cancer cell regions were detected using an adaptive binary threshold, and the rectangular shape-based regions were marked as the highest thermal conductivity and heat capacity (Cp) regions. Compared with traditional algorithms, the

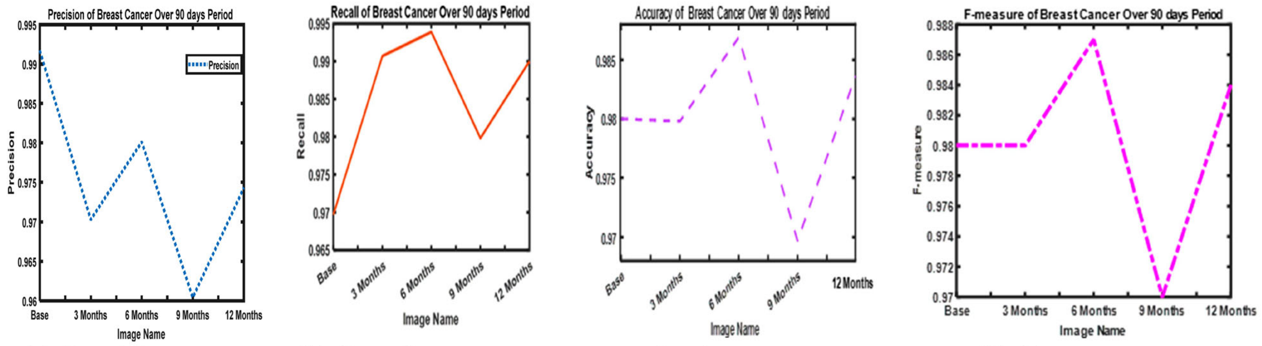

(a). Precision (b). Recall ©. Accuracy (d). F-measure

Figure 12. Breast Cancer Precision, Recall, Accuracy and F1-measure of 90 days Period.

Table 3. Statistical Analysis of base, 3, 6, 9 and 12 Months heat amplified cancer cell.

Image	TP	TN	FP	FN	Precision	Recall	Accuracy	F-measure	TPR	FPR
Base	480	491	4	15	0.9917	0.9697	0.98	0.98	0.9697	0.0081
3 Months	490	480	15	5	0.9703	0.9907	0.9798	0.98	0.9899	0.0303
6 Months	492	485	3	10	0.9801	0.9939	0.9869	0.987	0.9939	0.0202
9 Months	485	475	10	20	0.9604	0.9798	0.9697	0.97	0.9798	0.0404
12 Months	492	482	3	13	0.9743	0.99	0.9838	0.9840	0.9939	0.0263

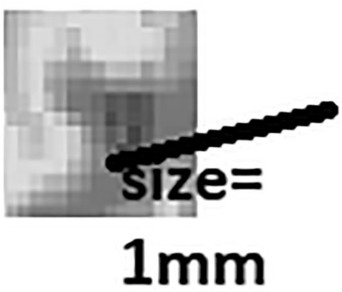

Figure 13. Size of breast cancer.

Table 4. Tumour size and stage.

Stage	Size
T1mi	1mm
T1a	> 1 mm and < 5 mm
T1b	> 5 mm and < 10 mm
T1c	> 10 mm and < 20 mm

Table 5. Comparision of differernt imaging modalities with different patients.

Patient	Methodology	cancer size detection
Patient 1 [34]	Mammography	> 20 mm
Patient 2 [34]	Mammography	40 mm
Patient 3 [35]	Magnetic Resonance Imaging	22.53 mm
Patient 4 [36]	Clinical Examination	12.17 mm
Patient 5 [37]	PET	20 mm
Patient 6(Proposed MWTDnCNN)	Thermogram Image	1 mm

proposed method achieves an accuracy of 98%. Furthermore, the method can be extended with magnetic amplification of cancer cells and detection of T1 cancer cells.

Table 6. Comparison of breast cancer detection.

Algorithm /methods	Accuracy	Precision	Recall
CNN [33]	0.854	0.842	0.88
Deep CNN [38]	0.958	0.94	0.92
Deep CNN with Attention Mechanism [39]	0.993	0.96	0.94
VGG 16 [40]	0.83	0.84	0.86
Unet +2 class CNN [41]	0.993	0.98	0.96
HOG [42]	0.958	0.946	0.954
Statistical [43]	0.901	0.90	0.91
Texture [44]	0.795	0.797	0.798
MWTDnCNN (Proposed method)	0.98	0.99	0.9743

Acknowledgements

The authors thank Dr. V. M. Duraimavalavan, Oncologist from SRM Medical College and Research Centre, supported Ethical Clearance. The authors thank Dr. N. R. Shanker supported laboratories.

Disclosure statement

No potential conflict of interest was reported by the author(s).

Ethical clearance

Got ethical clearance for this study from SRM Medical College Hospital and Research Centre, Chennai 603203, India.

References

[1] Weiss A, Chavez-MacGregor M, Lichtensztajn DY, et al. Validation study of the American joint committee on cancer eighth edition prognostic stage compared with the anatomic stage in breast cancer. JAMA Oncol. 2018;4(2):203–209. doi:10.1001/jamaoncol.2017.4298

[2] Ratanachaikanont T. Clinical breast examination and its relevance to diagnosis of palpable breast lesion; 2005. [Online]. Available from: http://www.medassocthai.org/journal

[3] Herranz M, Ruibal A. Optical imaging in breast cancer diagnosis: The next evolution. J Oncol. 2012;1:1–10. doi:10.1155/2012/863747.

[4] El-Gamal FEZA, Elmogy M, Atwan A. Current trends in medical image registration and fusion. Egypt Inform J. 2016;17(1):99–124. doi:10.1016/j.eij.2015.09.002. Elsevier B.V.

[5] Kapur A, Carson PL, Eberhard J, et al. Combination of digital mammography with semi-automated 3D breast ultrasound [Online]. Available: www.tcrt.org

[6] Berberoğlu K. Use of positron emission tomography/computed tomography in radiation treatment planning for lung cancer. Mol Imaging Radionucl Ther. 2016;25(2):50–62. doi:10.4274/mirt.19870

[7] Breast Screening for Cancer- New advanced thermal evaluation - Apollo Clinic Blog.

[8] Thermography Center of Memphis: Blog - Thermography Center of Memphis (memphisthermography.com)

[9] Rakhunde MB, Gotarkar S, Choudhari SG. Thermography as a breast cancer screening technique: a review article. Cureus. 2022;14(11):e31251. doi:10.7759/cureus.31251

[10] Mammoottil MJ, Kulangara LJ, Cherian AS, et al. Detection of breast cancer from five-view thermal images using convolutional neural networks. J Healthc Eng. 2022;2022:4295221. doi:10.1155/2022/4295221

[11] Resmini R, da Silva LF, Medeiros PRT, et al. A hybrid methodology for breast screening and cancer diagnosis using thermography. Comput Biol Med. 2021;135:104553. ISSN 0010-4825. doi:10.1016/j.compbiomed.2021.104553

[12] Sánchez-Cauce R, Pérez-Martín J, Luque M. Multi-input convolutional neural network for breast cancer detection using thermal images and clinical data. Comput Methods Programs Biomed. 2021;204:106045. doi:10.1016/j.cmpb.2021.106045

[13] Gonzalez-Hernandez J-L, Recinella AN, Kandlikar SG, et al. An inverse heat transfer approach for patient-specific breast cancer detection and tumor localization using surface thermal images in the prone position; 2020.

[14] Min S, et al. Thermal infrared image analysis for breast cancer detection. KSII Trans Internet Inf Syst. 2017;11(2):1134–1147. doi:10.3837/tiis.2017.02.029

[15] Yadav SS, Jadhav SM. Thermal infrared imaging based breast cancer diagnosis using machine learning techniques. Multimed Tools Appl. 2022;81(10):13139–13157. doi:10.1007/s11042-020-09600-3

[16] Abo El-Soud MW, Eltoukhy MM. Breast cancer detection in thermal images using extreme learning machine. J Intell Fuzzy Syst. 2020;38(3):2673–2681. doi:10.3233/JIFS-179553

[17] Ekici S, Jawzal H. Breast cancer diagnosis using thermography and convolutional neural networks. Med Hypotheses. 2020;137:109542. doi:10.1016/j.mehy.2019.109542

[18] Alnowami MR, Abolaban FA, Taha E. A wrapper-based feature selection approach to investigate potential biomarkers for early detection of breast cancer. J Radiat Res Appl Sci. 2022;15(1):104–110. doi:10.1016/j.jrras.2022.01.003

[19] Mukhmetov O, Igali D, Mashekova A, et al. Thermal modeling for breast tumor detection using thermography. Int J Therm Sci. 2021;161:106712. doi:10.1016/j.ijthermalsci.2020.106712

[20] Dey S, Roychoudhury R, Malakar S, et al. Screening of breast cancer from thermogram images by edge detection aided deep transfer learning model. Multimed Tools Appl. 2022;81(7):9331–9349. doi:10.1007/s11042-021-11477-9

[21] Macedo M, Santana M, dos Santos WP, et al. Breast cancer diagnosis using thermal image analysis: a data-driven approach based on swarm intelligence and supervised learning for optimized feature selection. Appl Soft Comput. 2021;109:107533. doi:10.1016/j.asoc.2021.107533

[22] Mambou SJ, Maresova P, Krejcar O, et al. Breast cancer detection using infrared thermal imaging and a deep learning model. Sensors. 2018;18(9):2799. doi:10.3390/s18092799

[23] Ghayoumi Zadeh H, Montazeri A, Abaspur Kazerouni I, et al. Clustering and screening for breast cancer on thermal images using a combination of SOM and MLP. Comput Methods Biomech Biomed Eng Imaging Vis. 2017;5(1):68–76. doi:10.1080/21681163.2014.978896

[24] Lashkari A, Pak F, Firouzmand M. Breast thermal images classification using optimal feature selectors and classifiers. J Eng. 2016;2016(7):237–248. doi:10.1049/joe.2016.0060

[25] Vysochanska S. Thermal characterization of infrared images for breast cancer thermal characterization of infrared images for breast cancer detection [Online]. Available from: https://scholarworks.rit.edu/theses

[26] Lozano A, Hayes JC, Compton LM, et al. Determining the thermal characteristics of breast cancer based on high-resolution infrared imaging, 3D breast scans, and magnetic resonance imaging. Sci Rep. 2020;10(1):105–119. doi:10.1038/s41598-020-66926-6

[27] Razmjooy N, Sheykhahmad FR, Ghadimi N. A hybrid neural network - World Cup optimization algorithm for melanoma detection. Open Med. 2018;13:9–16. doi:10.1515/med-2018-0002

[28] Parsian A, Ramezani M, Ghadimi N. A hybrid neural network-gray wolf optimization algorithm for melanoma detection. Biomed Res. 2017;28(8):3408–3411.

[29] Xu Z, Sheykhahmad FR, Ghadimi N, et al. Computer-aided diagnosis of skin cancer based on soft computing techniques. Open Med. 2020;15(1):860–871. doi:10.1515/med-2020-0131

[30] Mehrpooya M, Ghadimi N, Marefati M, et al. Numerical investigation of a new combined energy system includes parabolic dish solar collector, Stirling engine and thermoelectric device. Int J Energy Res. 2021;45(11):16436–16455. doi:10.1002/er.6891

[31] Ye H, Jin G, Fei W, et al. High step-up interleaved dc/dc converter with high efficiency. Energy Sources Part A. 2024;46(1): 4886–4905. doi:10.1080/15567036.2020.1716111

[32] Mishra S, Prakash A, Roy SK, et al. Breast cancer detection using thermal images and deep learning. In 2020 7th International Conference on Computing for Sustainable Global Development (INDIACom), New Delhi, India; 2020. p. 211–216. doi:10.23919/INDIACom49435.2020.9083722

[33] Alshehri A, AlSaeed D. Breast cancer detection in thermography using convolutional neural networks (CNNs) with deep attention mechanisms. Appl Sci. 2022;12(24):12922. doi:10.3390/app122412922

[34] Welch HG, Prorok PC, O'Malley AJ, et al. Breast-cancer tumor size, overdiagnosis, and mammography screening effectiveness. N Engl J Med. 2016;375(15):1438–1447. doi:10.1056/NEJMoa1600249

[35] Haddad M, Xu B, Pun C, et al. Breast specimen measurement methodology and its potential major impact on tumor size. Int J Surg Pathol. 2021;29(1):39–45. doi:10.1177/1066896920962184
[36] Cortadellas T, Argacha P, Acosta J, et al. Estimation of tumor size in breast cancer comparing clinical examination, mammography, ultrasound and MRI—correlation with the pathological analysis of the surgical specimen. Gland Surg. 2017;6(4):330. doi:10.21037/gs.2017.03.09
[37] Kuroda H, Yoshizako T, Yada N, et al. Exploration of tumor size measurement methods in preoperative breast cancer assessment using whole-body silicon photomultiplier PET: feasibility and first results. Jpn J Radiol. 2024;42(6):639–647. doi:10.1007/s11604-024-01533-3
[38] Chatterjee S, Biswas S, Majee A, et al. Breast cancer detection from thermal images using a Grunwald-Letnikov-aided dragonfly algorithm-based deep feature selection method. Comput Biol Med. 2022;141:105027. ISSN 0010-4825. doi:10.1016/j.compbiomed.2021.105027
[39] Mohamed EA, Rashed EA, Gaber T, et al. Deep learning model for fully automated breast cancer detection system from thermograms. PLoS One. 2022;17(1):e0262349. doi:10.1371/journal.pone.0262349. Editor: Robertas Damasˇevičius,Politechni.
[40] Joyce JM. Kullback-Leibler divergence. In: Lovric M, editor. International encyclopedia of statistical science. Berlin: Springer; 2011. p. 720–722. doi:10.1007/978-3-642-04898-2_327
[41] Zhang K, Zuo W, Chen Y, et al. Beyond a Gaussian denoiser: residual learning of deep CNN for image denoising. IEEE Trans Image Process. 2017;26(7):3142–3155. doi:10.1109/TIP.2017.2662206
[42] Abdel-Nasser M, Moreno A, Puig D. Breast cancer detection in thermal infrared images using representation learning and texture analysis methods. Electronics (Basel). 2019;8(1):100. doi:10.3390/electronics8010100
[43] Silva LF, Sequeiros GO, Santos MLO, et al. Thermal signal analysis for breast cancer risk verification. Stud Health Technol Inform. 2015;216:746–750. doi:10.3233/978-1-61499-564-7-746
[44] Schaefer G, Závišek M, Nakashima T. Thermography based breast cancer analysis using statistical features and fuzzy classification. Pattern Recognit. 2009;42(6):1133–1137. doi:10.1016/j.patcog.2008.08.007